

Structure of Tl Adlayers on the Pt(111) Electrode Surface: Effects of Solution pH and Bisulfate Coadsorption

R. R. Adžić* and J. X. Wang

Department of Applied Science, Chemical Sciences Division, Brookhaven National Laboratory, Upton, New York 11973

O. M. Magnussen and B. M. Ocko

Department of Physics, Brookhaven National Laboratory, Upton, New York 11973

Received: January 2, 1996; In Final Form: May 19, 1996[⊗]

The structure of Tl adlayers deposited at underpotentials on Pt(111) has been investigated in four different electrolyte solutions (HClO₄, NaClO₄, NaOH, and H₂SO₄) with surface X-ray scattering (SXS) techniques. In all solutions investigated, Tl forms an incommensurate, aligned-hexagonal phase at the most negative potentials prior to its bulk deposition or hydrogen evolution. With decreasing potential the monolayer compresses and thus the Tl coverage increases. Under hydrogen evolution, the close-packed hexagonal Tl monolayer also exists and this reaction causes a slight lowering of the Tl coverage and a significant decrease of the in-plane ordering of the monolayer. In sulfuric acid solution, besides the close-packed hexagonal phase, a commensurate ($\sqrt{3} \times \sqrt{3}$)R30° phase with a Tl coverage of $1/3$ monolayer is formed in coadsorption with bisulfates over a 0.22 V wide potential range.

I. Introduction

Electrochemical formation of metal monolayers by so-called underpotential deposition (UPD) involves deposition of up to 1 or 2 monolayers of a metal onto a different substrate at potentials more positive than the deposition potential of the bulk metal. It has been the subject of numerous recent *in situ* structural studies. Most of these studies involved Ag and Au as the substrate metals, such as for UPD of Tl.^{1–4} Platinum, as a transition metal element, is chemically more active than Au and Ag and its modification by UPD adlayers has rather unique electrocatalytic properties, which have attracted considerable attention.⁵ Distinct adlayer structures have been observed on Pt(111) compared to that on the silver and gold (111) surfaces. Lead, for instance, forms commensurate monolayers on Pt(111)⁶ while it forms an incommensurate hexagonal monolayer on Ag(111) and Au(111).⁷ In this work, the structure of Tl monolayers on Pt(111) is determined and compared to those on Au(111) and Ag(111).

Of particular interest is that the large Tl UPD potential range overlaps with the potential region for hydrogen adsorption/evolution on Pt in acid and neutral solutions. In the past, the effect of adsorbates on hydrogen adsorption, evolution, and absorption at metal electrodes has been extensively studied via a variety of electrochemical and spectroscopic techniques. However, in most instances the adlayer structure and coverage have not been determined under reaction conditions, although this information is very important for understanding the adlayer effects. We report here the structure and coverage of the Tl monolayer as a function of potential in acid, neutral, and alkaline solutions. The results not only provide accurate structural information but also reveal the solution pH effects on the coverage and the phase behavior of the Tl adlayers.

Another interesting aspect of Tl/Pt(111) is anion coadsorption. The first observation of anion coadsorption in an UPD system was reported by Horanyi et al. for sulfate and chloride

coadsorption with a copper adlayer on platinum using radiotracer techniques.⁸ In electrochemical–UHV studies of copper adsorption on I₂-prepared Pt(111) several Cu–I structures have been found.⁹ The effects of anions on the structure of copper adlayers on Au low index surfaces^{10,11} and on Pt(111)¹² and silver adlayers on Au(111)¹³ have been studied by *in situ* scanning probes and SXS techniques. Besides copper, sulfate chemisorption was reported for the cadmium adlayer on Pt¹⁴ and hydroxide ion coadsorption with Tl on Au(111).³ In a recent note, pronounced effects of specifically adsorbed anions on the UPD of Tl on Pt(111) were reported.¹⁵ In this paper, the thallium and anion coadsorbed adlayer structure observed in sulfuric acid solution are reported.

II. Experimental Section

A platinum single crystal, obtained from Metal Crystals and Oxides Ltd., Cambridge, England, was oriented within 0.2° of the <111> crystallographic direction and polished by using diamond paste with a final polishing using 1 micron particles. The crystal was annealed in a propane flame, cooled in a hydrogen stream, and subsequently transferred to the electrochemical X-ray scattering cell protected by a drop of the solution. The cell was constructed from Kel-F¹⁶ and sealed using a 4 μm thick Prolene (Chemplex Inc.) X-ray window. The solutions were prepared from Tl₂CO₃ (Aldrich), NaClO₄, NaOH, HClO₄ (Merck, Suprapur), and Milli-Q water (Millipore Inc.). Ultrapure nitrogen was used to deoxygenate the solutions. The counter electrode was platinum, while a reversible hydrogen electrode served as the reference. All potentials are given with respect to normal hydrogen electrode (NHE).

SXS measurements were carried out at the National Synchrotron Light Source (NSLS) at beam line X22B and X22A with $\lambda = 1.54$ and 1.20 Å, respectively. A full description of the electrochemical SXS technique has been presented elsewhere.¹⁶ For in-plane diffraction measurements, the resolution was determined primarily by a 3 mrad Soller slit on the detector arm. This arrangement provides a 2θ resolution of 0.1° half-width at half-maximum (hwhm). For specular reflectivity

[⊗] Abstract published in *Advance ACS Abstracts*, August 1, 1996.

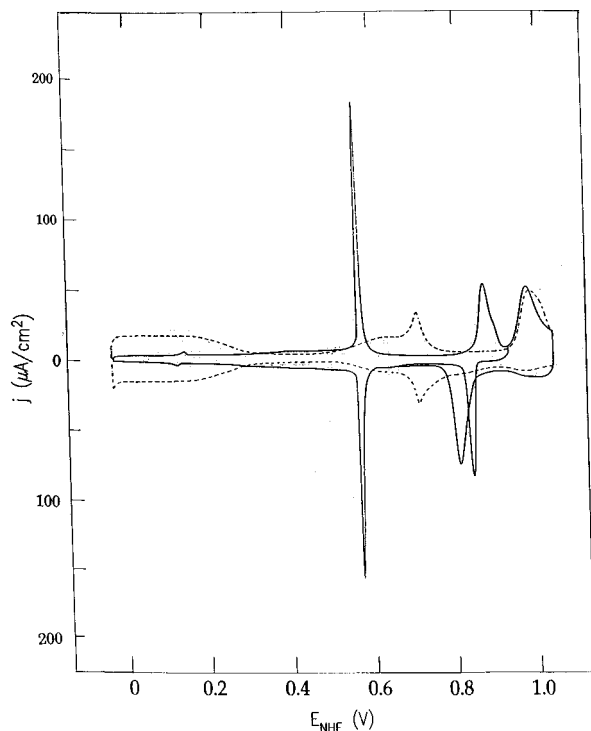


Figure 1. Voltammetry curve for Tl monolayer deposition at underpotentials on Pt(111) in 0.1 M HClO₄ solution containing 1 mM Tl⁺ with two different positive potential limits. Sweep rate 20 mV/s. Dashed line is the curve for Pt(111) obtained in the absence of Tl⁺ in solution.

measurements, a 2 mm wide slit was used in the scattering plane which has an acceptance of 3 mrad. The transverse in-plane resolution was limited by the mosaic spread of the platinum single crystal which is about 0.07° hwhm. For Pt(111), it is convenient to use a hexagonal coordinate system in which $Q = (a^*, b^*, c^*) \cdot (H, K, L)$, where $a^* = b^* = 4\pi\sqrt{3}a = 2.614 \text{ \AA}^{-1}$, $c^* = 2\pi/\sqrt{6}a = 0.924 \text{ \AA}^{-1}$, and $a = 2.775 \text{ \AA}$. The in-plane diffraction measurements were carried out in the (H, K) plane with $L = 0.2$ corresponding to a grazing incident angle of 1.25°.

III. Results and Discussion

A. Voltammetry of the UPD of Tl on Pt(111). Figure 1 displays the voltammetry curve for the UPD of Tl on Pt(111) in 0.1 M perchloric acid solution (solid line) and the curve for Pt(111) in perchloric acid without Tl⁺ (dashed line). Complete desorption of Tl takes place at 0.86 V, before the PtOH formation of 0.97 V. This is inferred from a negligible difference between the anodic peaks at 0.97 V in the absence and in the presence of Tl. The UPD commences with the cathodic peak at 0.83 V. The pair of peaks at 0.57 V is due to a surface process, which can be inferred from their reversibility. At more negative potentials, a small UPD current is seen up to the onset of hydrogen evolution. The charge from -0.03 to 0.9 V, after subtracting the double layer charge current for Pt(111) in the absence of Tl, amounts of $206 \mu\text{C cm}^{-2}$. This is about $60 \mu\text{C cm}^{-2}$ larger than the charge required for a deposition of a hexagonal close-packed monolayer of Tl assuming one electron per Tl adatom. The excess charge may be caused by the difference in the double layer charging current in the solutions with and without Tl.

Figure 2 shows the UPD of Tl in 0.05 M H₂SO₄ solution (solid line) and the curve without Tl⁺ (dashed line) is given for comparison. In comparison with the curve in the presence of nonadsorbing perchlorate anions (Figure 1), the presence of

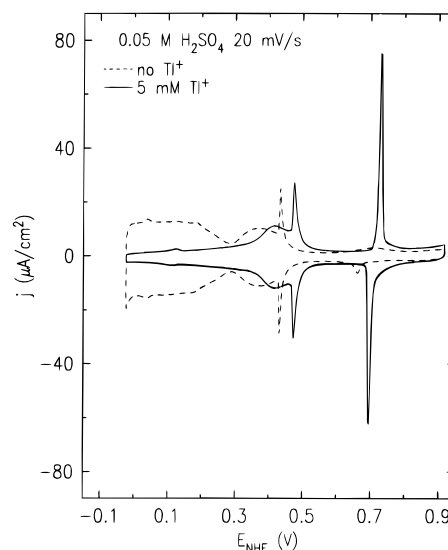


Figure 2. Voltammetry curve for Tl monolayer deposition at underpotentials on Pt(111) in 0.05 M H₂SO₄ solution containing 5 mM Tl⁺. Sweep rate 20 mV/s. Dashed line is the curve for Pt(111) obtained in the absence of Tl⁺ in solution.

sulfate/bisulfate in solution causes a 0.14 V shift of the UPD peak at 0.83 V to a more negative potential and a disappearance of the pair of peaks at 0.57 V. A new pair of broad peaks occur at 0.42 V which merge with the sharp, reversible peaks at 0.48 V. The similarity of this pair of peaks and the peaks observed for sulfate adsorption on Pt(111)¹⁷ is noteworthy. Clavilier et al.¹⁸ ascribed these peaks to the reaction of Tl⁺ or H⁺. We propose the Tl-bisulfate coadsorption to be associated with these peaks on the basis of the above-mentioned similarity and the fact that these features do not exist in HClO₄ solution (cf. Figure 1). Most recently, the coadsorption of bisulfate and Tl in this potential region was shown by *in situ* FTIR.¹⁹ The charge from -0.03 to 0.93 V is $153 \mu\text{C cm}^{-2}$, significantly smaller than the charge in HClO₄. The determination of the charge for Tl in this solution is particularly difficult due to anion coadsorption in a wide potential region and to the uncertainty in subtracting the double layer charging current for Pt. The positive potential limit of the Tl desorption is not clearly seen which may be the source of error in calculating the charge. A more detailed discussion on the voltammetry of the Tl UPD in acid solutions was previously reported.¹⁵

Figure 3 shows the voltammetry curves obtained in 0.1 M sodium hydroxide solutions in the presence and in the absence of Tl. The potential region of the Tl UPD in this alkaline solution is smaller than in the other acid solutions investigated because of the limits determined by the bulk Tl deposition at negative potentials and the Pt oxide formation at positive potentials. Since hydrogen adsorption and hydrogen evolution in this solution are shifted to potentials negative of the bulk Tl deposition potential, there is no overlap of these reactions with the UPD of Tl. Consequently, the voltammetry of the UPD of Tl is not affected by hydrogen adsorption/evolution. The major Tl UPD peak, however, occurs at more negative potential (around -0.1 V) than in acid solutions and probably involves the adsorption/desorption of OH⁻. The PtOH formation peak is shifted to more positive potentials in comparison with the peak in the absence of Tl⁺. Note the difference in the sweep rates for the two curves in Figure 3.

B. Structure of Tl Adlayers. 1. Perchloric Acid, Sodium Perchlorate, and Sodium Hydroxide Solutions. Grazing incident X-ray diffraction measurements were used to determine the structure of close-packed Tl monolayers, the potential, and

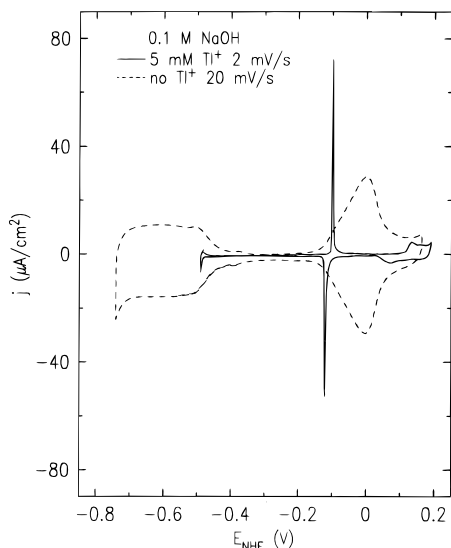


Figure 3. Voltammogram curve for Tl monolayer deposition at underpotentials on Pt(111) in 0.1 M NaOH solution containing 5 mM Tl^+ . Sweep rate 2 mV/s. Dashed line is the curve for Pt(111) obtained in the absence of Tl^+ in solution at the sweep rate of 20 mV/s.

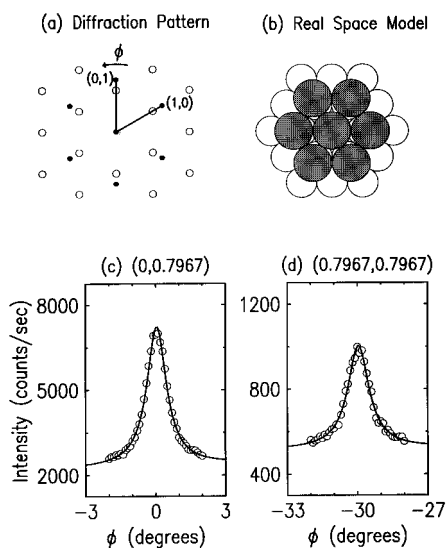


Figure 4. (a) In-plane diffraction patterns for Tl/Pt(111) at -0.23 V in 0.1 M NaClO_4 containing 5 mM Tl^+ . The solid and open circles represent the diffraction pattern for Pt(111) and from the aligned-hexagonal Tl monolayers, respectively. (b) Real space model of Tl monolayer on Pt(111) derived from (a). (c) and (d) Azimuthal scans through the low-order diffraction peaks of the Tl monolayer in the aligned-hexagonal phase, where $\phi = 0$ corresponds to the $\langle 01 \rangle$ axis.

solution pH dependent phase behavior. The results obtained from the 0.1 M NaClO_4 solution containing 5 mM Tl^+ are described first since the ordered Tl monolayer exists over the largest potential region in neutral solutions. Subsequently, the effects of OH^- coadsorption, solution pH, and hydrogen evolution are demonstrated by the data obtained from the NaOH and HClO_4 solutions containing the same amount of Tl^+ .

Figure 4a shows the in-plane diffraction pattern observed at -0.23 V in 0.1 M NaClO_4 solution. Besides the reflections from the Pt(111) substrate, which are given by solid dots, additional reflections (open circles) are observed which have a hexagonal symmetry and are aligned with the substrate. The real space model deduced from this diffraction pattern is shown in Figure 4b. Figure 4c,d shows azimuthal scans through the (0, 0.7967) and the (0.7967, 0.7967) positions which have a hwhm peak width of 0.5° . This is significantly broader than the peak width of 0.1° found for the (01) substrate peak. These

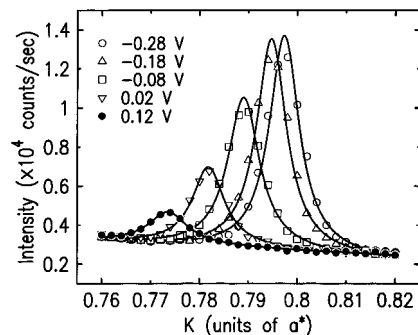


Figure 5. Diffraction scans along the K direction through one of the lowest-order diffraction peaks ($H = 0$) of the aligned-hexagonal Tl monolayer in 0.1 M NaClO_4 with 5 mM Tl^+ as a function of potential. Solid lines are the fits to the Lorentzian line shape.

two peaks indicate that the adlayer is aligned hexagonal rather than rectangular.

In order to determine the phase behavior of the aligned hexagonal Tl monolayer, the diffraction intensity profile at the lowest-order position was monitored as a function of potential starting at -0.28 V, which is prior to hydrogen evolution. Diffraction scans along the K direction at $H = 0$ were taken before each 0.05 V potential increment. Several scans shown in Figure 5 illustrate how the diffraction peak position and intensity vary with potential. At all potentials, the diffraction peaks are well described by Lorentzian profiles, shown as the solid lines. The peak, whose center is defined by the reciprocal lattice constant, τa^* , shifts to smaller K as the potential increases. Since the coverage, relative to the substrate, equals to τ^2 , the coverage decreases with increasing potential. At potentials negative of 0.07 V, the peak width has a constant value of 0.010 \AA^{-1} hwhm. This width corresponds to a coherence length (i.e., the average domain size) of 100 \AA . The diffracted intensity decreases with decreasing coverage. It completely vanishes above 0.17 V. In the whole potential range, the Tl adlayer remains aligned with the substrate.

In 0.1 M NaOH and HClO_4 electrolytes, the same aligned-hexagonal diffraction pattern was observed. However, the Tl coverages, diffracted intensities, and phase transition potential are different in the three solutions. Figure 6 shows the Tl coverage and lattice constant ($a_{\text{Tl}} = a/\tau$) as a function of potential obtained from the three solutions. Since perchlorate coadsorption with Tl on Pt(111) does not occur below 0.3 V,¹⁹ the observed differences at potentials below 0.2 V are attributed to the effect of solution pH. To avoid the uncertainties in pH within the thin solution layer due to hydrogen evolution, the measurements in acid and neutral solutions were limited to the potentials prior to hydrogen evolution. A continuous decrease of coverage or increase of the Tl lattice spacing with increasing potential occurs in all the solutions. Fits of a quadratic function to the data are shown by the solid lines.

In alkaline solution, a maximum coverage of 0.67 is reached at the most negative potential prior to Tl bulk deposition. With increasing potential, the Tl coverage decreases as the hexagonal lattice expands. The hexagonal structure vanishes around -0.1 V corresponding to the major current peak in the voltammogram (cf. Figure 3). This is probably related to the OH^- chemisorption.

In neutral and acid solutions the hexagonal phase vanishes at about 0.2 and 0.1 V, respectively. Since the OH^- adsorption shifts by about 0.4 V from -0.1 to 0.3 V for the pH change from 13 to 6, the loss of order is not related to OH^- adsorption. In both solutions, the diffraction intensity from the adlayer decreases considerably with increasing potential above 0 V. This

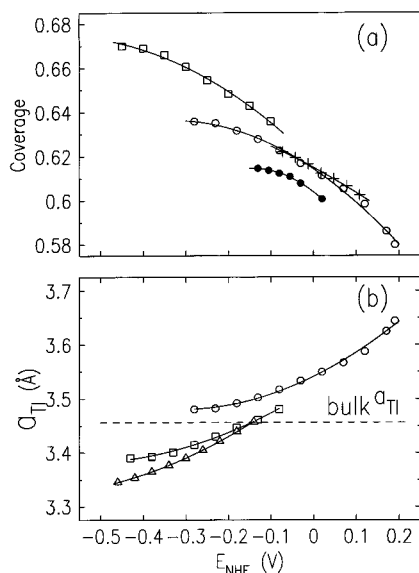


Figure 6. Tl Coverage (a) and hexagonal lattice constant (b) as a function of potential. All the solutions contains 5 mM Tl⁺ and 0.1 M NaOH (squares), NaClO₄ (circles), HClO₄ (plus signs), respectively. The solid lines are the quadratic fits to the data. All the data were taken in positive potential increments except for the 1 M HClO₄ data (solid circles) which were taken in negative potential increments to minimize the accumulation of hydrogen gas in the cell from hydrogen evolution. The Tl lattice spacing on Au(111) in 0.1 M HClO₄ with 5 mM Tl⁺ is shown by the triangles in (b) for comparison. The bulk a_{Tl} is the in-plane lattice constant of a hcp-Tl crystal.

can be attributed to the decrease of long-range order as the Tl lattice constant (see Figure 6b), i.e., the nearest-neighbor-separation, becomes significantly larger than that for bulk Tl. The diffraction intensity also decreases with increasing the acidity of the solution (from pH = 6 to pH = 0) at potentials around 0 V. This appears to be the reason for the loss of the diffraction signal at a less positive potential in acid solution than that in neutral solution. The Tl coverage is essentially the same at negative potentials but is slightly different at positive potentials in these two solutions.

For neutral and alkaline solutions, significant differences in coverage appear at potentials negative of -0.1 V. Adsorption of OH⁻ in alkaline solution in this potential region cannot be the cause of this difference since the difference increases, while the OH⁻ adsorption should decrease, with decreasing potential. Besides this, the coverages in alkaline solution are higher than that in neutral solution at the same potentials. It is unlikely that OH⁻ coadsorption can make a close-packed Tl monolayer more compressed.

In order to further elucidate the effect of solution pH on the Tl monolayer and determine the structure and coverage of the Tl adlayer during hydrogen evolution, X-ray diffraction measurements were carried out in 1 M HClO₄ solution containing 5 mM Tl⁺. At about 0.0 V, the Tl coverage is considerably lower (as shown in Figure 6a) and the scattered intensity is weaker in this solution compared to those in 0.1 M HClO₄. Consequently, the positive potential limit for the hexagonal phase is decreased from 0.12 to 0.03 V. Below -0.05 V, the hydrogen evolution current rises quickly with decreasing potential. Under the reaction condition, the hexagonal Tl monolayer structure is stable but its compressibility decreases. The measurements at potentials below -0.15 V are difficult because hydrogen bubbles form in the thin layer cell.

The behavior of the hexagonal Tl monolayer in solutions of various pH is distinctly different from the behavior of the Tl/Au(111) system. For the latter system, Tl shifts the measurable

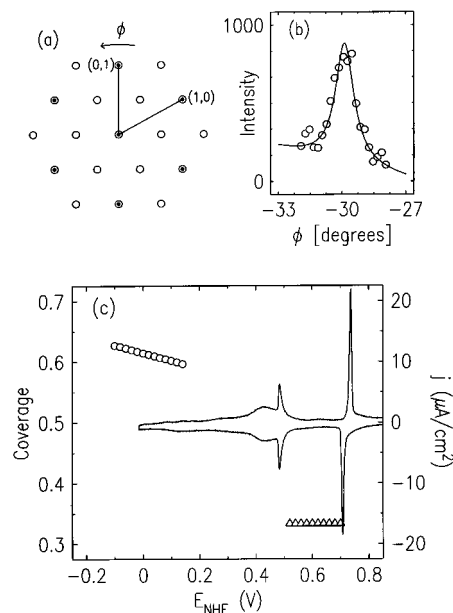


Figure 7. (a) In-plane diffraction patterns for Tl/Pt(111) at 0.7 V in 0.05 M H₂SO₄ solution containing 5 mM Tl⁺. The solid and open circles represent the diffraction pattern from Pt(111) and from the ($\sqrt{3} \times \sqrt{3}$)R30° adlayer, respectively. (b) Azimuthal scans through the (1/3, 1/3) position. The solid line is the fit to the Lorentzian line shape. (c) Tl coverages of the aligned-hexagonal and ($\sqrt{3} \times \sqrt{3}$)R30° phases as a function of potential and the voltammogram in 0.05 M H₂SO₄ solution with 5 mM Tl⁺. Sweep rate 5 mV/s.

currents of hydrogen evolution by at least -0.4 V to potentials negative of bulk Tl deposition. It appears that for this reason the Tl lattice spacing (Figure 6b) and the diffraction intensity are independent of solution pH. Further studies are required for a complete understanding of the solution pH effect on the coverage of Tl monolayer on Pt(111).

2. Sulfuric Acid Solution. An incommensurate, aligned-hexagonal Tl phase has also been observed in sulfuric acid solution from -0.1 to 0.14 V with the coverage ranging from 0.635 to 0.590 (see Figure 7c) similar to that in perchloric acid solution. In both solutions, the positive potential limit corresponds to a very small peak in voltammetry (cf. Figures 1 and 2) showing that only a small discontinuous decrease in Tl coverage is associated with the phase transition. A search for high-order commensurate structures with medium coverage was carried out above 0.14 V in sulfuric acid solution. Weak diffraction peaks were observed around 0.2 V at the (4/7, 2/7) and (2/7, 8/7) positions in one of the three experiments. The corresponding 4Tl-($\sqrt{7} \times \sqrt{7}$) structure gives a coverage of 0.57 (=4/7). The difficulty in observing this phase may be due to the small domain sizes. Further studies with other techniques that can detect the structures of small domain sizes are required in this potential region.

Above 0.48 V, where a sharp peak in the voltammetry curve occurs (Figure 7c), diffraction peaks were observed at (1/3, 1/3) and (2/3, 2/3) positions. From these observations the ($\sqrt{3} \times \sqrt{3}$)R30° diffraction pattern, as shown in Figure 7a, was deduced. Figure 7b shows the azimuthal scan through the (1/3, 1/3) peak which has a hwhm of 0.54°. The hwhm in the radial scan is 0.012 Å⁻¹. Both are slightly wider than those for the hexagonal Tl monolayer. The diffraction intensity at the (1/3, 1/3) position was monitored in a positive potential sweep. It exists between 0.50 and 0.72 V (both potentials correspond to the diffraction intensity at the half of the maximum value). This potential range corresponds to the

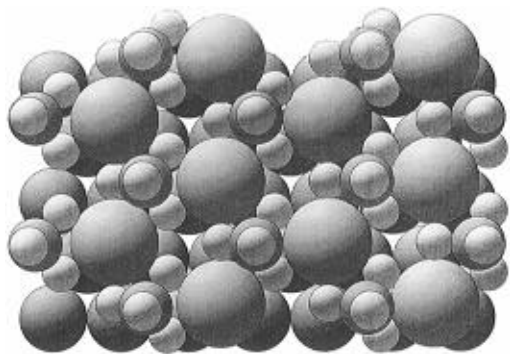


Figure 8. Proposed real space model for the $(\sqrt{3} \times \sqrt{3})R30^\circ$ Tl – HSO_4^- coadsorbed adlayer on Pt(111).

potential between the two major anodic peaks in the voltammogram as shown in Figure 7c.

The involvement of both Tl and anion species in the $(\sqrt{3} \times \sqrt{3})R30^\circ$ lattice structure can be inferred from the absence of the $(1/3, 1/3)$ signal in the solutions without either Tl^+ or sulfate/bisulfate. In addition, the bisulfate coadsorption with Tl on Pt(111) was clearly demonstrated by *in situ* FTIR measurements.¹⁹ The large size of Tl rules out the honeycomb lattice of Tl adatoms with a $2/3$ monolayer coverage. (As presented in the previous subsection, a $2/3$ monolayer is in fact the maximum Tl coverage found in the close-packed hexagonal phase.) From analysis of the specular reflectivity profile (not presented here), the Tl–Pt layer spacing was found to be $2.42 \pm 0.05 \text{ \AA}$. This gives a Tl–Pt bond length of 2.90 \AA for Tl in the threefold hollow sites. This bond length is very close to the sum of the Pt and Tl covalent radii (2.84 \AA) which suggests a strong interaction between the Tl and Pt and supports the assumption that the Tl adatoms are in the hollow sites.

It is, however, difficult to determine the bisulfate coverage and its adsorption sites because the scattering from its low-Z atomic components is much weaker than that from Tl and Pt. The bisulfate adsorption (without Tl) and coadsorption (with Tl) features in the voltammograms are very similar (cf. Figure 2). The positive potential shift in the latter case indicates that the Tl adatoms impede the bisulfate adsorption. These facts suggest that bisulfate interacts with not only Tl but also Pt. Hence, the adsorption sites of the bisulfates are most probable the hollow sites of the Tl adlayer. The interaction between bisulfates and Tl adatoms was shown by FTIR.¹⁹ In the model shown in Figure 8, Tl, Pt, S, and O are represented by spheres corresponding to their relative atomic sizes. It can be seen that the model gives adequate interatomic spacings. Further studies are needed to verify the proposed model. For example, chronocoulometric²⁰ or rotating disc–ring²¹ measurements may provide information on bisulfate coverage and the scanning microscopic techniques may give a real space image of this adlayer.

IV. Conclusions

Tl forms ordered adlayers at underpotentials on Pt(111) in HClO_4 , NaClO_4 , NaOH , and H_2SO_4 solutions as revealed by SXS techniques. In all solutions investigated, Tl forms an incommensurate, aligned-hexagonal phase at the most negative potentials prior to its bulk deposition or hydrogen evolution. With decreasing potential the monolayer compresses, and thus the Tl coverage increases. The details of the behavior of this phase depend on the solution composition and pH. Under hydrogen evolution, the close-packed hexagonal Tl monolayer also exists and this reaction causes a slight lowering of the Tl

coverage and a significant decrease of the in-plane ordering of the monolayer. The cause of the coverage decrease of the hexagonal Tl monolayer on Pt(111) in solutions of increased acidity is difficult to identify from the existing data. It is likely that it may be a consequence of several effects. Specifically adsorbed anions have profound effects on the structure of low-coverage Tl adlayers. In sulfuric acid solution, besides the close-packed hexagonal phase, a commensurate $(\sqrt{3} \times \sqrt{3})R30^\circ$ phase with a Tl coverage of $1/3$ monolayer is formed in coadsorption with bisulfates over a 0.22 V wide potential range.

Acknowledgment. The authors thank S. Feldberg for useful discussions and D. Wheeler for his help with initial voltammetric study. This research was performed under the auspices of the U.S. Department of Energy, Divisions of Chemical and Materials Sciences, Office of Basic Energy Sciences, under Contract No. DE-AC02-76CH00016.

References and Notes

- (1) (a) Toney, M. F.; Gordon, J. G.; Kau, L.; Borges, G. L.; Melroy, O. R.; Samant, M. H.; Wiesler, D.; Yee, D.; Sorensen, L. *Phys. Rev. B* **1990**, *42*, 5594. (b) Toney, M. F.; Gordon, J. G.; Samant, M. H.; Borges, G. L.; Melroy, O. R.; Yee, D.; Sorensen, L. B. *Phys. Rev. B* **1992**, *45*, 9362.
- (2) Wang, J. X.; Adžić, R. R.; Magnussen, O. M.; Ocko, B. M. *Surf. Sci.* **1995**, *344*, 111.
- (3) (a) Wang, J. X.; Adžić, R. R.; Ocko, B. M. *J. Phys. Chem.* **1994**, *98*, 7182. (b) Adžić, R. R.; Wang, J.; Ocko, B. M. *J. Electrochim. Acta* **1995**, *40*, 83.
- (4) Wang, J. X.; Adžić, R. R.; Magnussen, O. M.; Ocko, B. M. *Surf. Sci.* **1995**, *335*, 120.
- (5) Adžić, R. R. In *Advances in Electrochemistry and Electrochemical Engineering*; Gerischer, H., Tobias, C. W., Eds.; Wiley-Interscience: New York, 1984; Vol. 13, pp 159–260.
- (6) Adžić, R. R.; Wang, J.; Vitus, C. M.; Ocko, B. M. *Surf. Sci. Lett.* **1993**, *293*, 876.
- (7) Toney, M. F.; Gordon, J. G.; Samant, M. G.; Borges, G. L.; Melroy, O. R.; Yee, D.; Sorensen, L. B. *J. Phys. Chem.* **1995**, *99*, 4733.
- (8) Horanyi, G.; Vertes, G. *J. Electroanal. Chem.* **1974**, *55*, 45.
- (9) Stickney, J.; Rosasco, S. and Hubbard, A. *J. Electroanal. Chem.* **1984**, *131*, 260.
- (10) (a) Manne, S.; Hansma, P. K.; Massie, J.; Elings, V. B.; Gewirth, A. A. *Science* **1991**, *251*, 183. (b) Magnussen, O. M.; Hotlos, J.; Nichols, R. J.; Kolb, D. M.; Behm, R. J. *Phys. Rev. Lett.* **1990**, *64*, 2929. (c) Magnussen, O. M.; Hotlos, J.; Beitel, G.; Kolb, D. M.; Behm, R. J. *J. Vac. Sci. Technol. B* **1991**, *9*, 969. (d) Moller, F.; Magnussen, O. M.; Behm, R. J. *Electrochim. Acta* **1995**, *40*, 1259. (e) Hotlos, J.; Magnussen, O. M.; Behm, R. J. *Surf. Sci.* **1995**, *335*, 129.
- (11) Toney, M. F.; Howard, J. N.; Richer, J.; Borges, G. L.; Gordon, J. G.; Melroy, O. R.; Yee, D.; Sorensen, L. B. *Phys. Rev. Lett.* **1995**, *75*, 4472.
- (12) (a) Matsumoto, H.; Oda, I.; Itaya, K. *J. Electroanal. Chem.* **1993**, *356*, 275. (b) Matsumoto, H.; Inukai, J.; Ito, M. *J. Electroanal. Chem.* **1994**, *379*, 223. (c) Markovic, N. M.; Gasteiger, H. A.; Lucas, C. A.; Tidswell, I. M.; Ross, P. N. *Surf. Sci.* **1995**, *335*, 91. (d) Tidswell, I. M.; Lucas, C. A.; Markovic, N. M.; Ross, P. N. *Phys. Rev. B* **1995**, *51*, 10205.
- (13) Chen, C-h.; Vesecky, S. M.; Gewirth, A. A. *J. Am. Chem. Soc.* **1992**, *114*, 451.
- (14) Warga, K.; Zelenay, P.; Horanyi, G.; Wieckowski, A. I. *Electroanal. Chem.* **1992**, *327*, 291.
- (15) Wheeler, D. R.; Wang, J. X.; Adžić, R. R. *J. Electroanal. Chem.* **1995**, *387*, 115.
- (16) Wang, J.; Ocko, B. M.; Davenport, A. J.; Isaacs, H. *Phys. Rev. B* **1992**, *46*, 10321.
- (17) Adžić, R. R.; Feddrix, F.; Nikolic, B. Z.; Yeager, E. B. *J. Electroanal. Chem.* **1992**, *341*, 287.
- (18) Clavilier, J.; Ganon, J-P.; Petit, M. J. *Electroanal. Chem.* **1989**, *265*, 231.
- (19) Marinkovic, N. S.; Faucett, R. W.; Wang, J. X.; Adžić, R. R. *J. Phys. Chem.* **1995**, *99*, 17490.
- (20) (a) Shi, Z.; Lipkowsky, J. J. *J. Electroanal. Chem.* **1994**, *365*, 303. (b) Shi, Z.; Lipkowsky, J. J. *J. Electroanal. Chem.* **1994**, *364*, 289.
- (21) Markovic, N. M.; Gasteiger, H. A.; Ross, P. N. *Langmuir* **1995**, *11*, 40.